The broad iron K emission line in the Seyfert 2 galaxy IRAS 18325 − 5926

K. Iwasawa,[1] A. C. Fabian,[1] R. F. Mushotzky,[2] W. N. Brandt,[1] H. Awaki[3] and H. Kunieda[4]

[1]*Institute of Astronomy, Madingley Road, Cambridge CB3 0HA*
[2]*Goddard Space Flight Center, Green Belt, MD 20771, USA*
[3]*Department of Physics, Kyoto University, Sakyo-ku, Kyoto 606-01, Japan*
[4]*Department of Astrophysics, Nagoya University, Chikusa-ku, Nagoya 464-01, Japan*

ABSTRACT
We report the detection of a very broad iron Kα emission line in the *ASCA* X-ray spectrum of the Seyfert 2 galaxy IRAS 18325 − 5926. The line is strong, with an equivalent width $EW = 500$–800 eV, and its profile is peaked at 6.9 keV and skewed down to 4 keV. The energy of the blue peak of the line is significantly higher than the rest-energy of 6.4 keV seen in many active galaxies, which is expected from an iron Kα line arising in cold matter. If the breadth and shift of the line energy are caused by Doppler and relativistic effects in a cold accretion disc about a black hole, then the disc has an intermediate inclination, $i = 40°$–$50°$. A plausible interpretation for the large equivalent width is a supersolar abundance of iron; this also accounts for the lack of a significant reflection hump. The line profile can also be explained by emission from highly ionized matter very close to the central object. However, the lack of a deep iron K absorption edge in the *Ginga* spectrum is inconsistent with this interpretation.

We verify that fast X-ray variability on a time-scale of 10^4 s is common in this object, using *ASCA* and *ROSAT* observations which are partially simultaneous. A study of spectral variability using combined *ASCA* and *ROSAT* PSPC data reveals that the X-ray flux change occurred mainly above 1 keV, and suggests a stable, or at least less-variable, component below 1 keV. It should lie outside the nuclear obscuration region.

Key words: accretion, accretion discs – galaxies: active – galaxies: individual: IRAS 18325 − 5926 – galaxies: Seyfert – X-rays: galaxies.

1 INTRODUCTION

The X-ray spectra of many active galactic nuclei (AGN), in particular Seyfert galaxies, show complex spectral features due to obscuration and reprocessing (Mushotzky, Done & Pounds 1993). Theoretical calculations (George & Fabian 1991; Matt, Fabian & Ross 1993; Ross & Fabian 1993; Życki & Czerny 1994) and X-ray spectral fits (Awaki et al. 1991; Nandra & Pounds 1994) are consistent with the idea that the Fe K line and the high-energy hump above 10 keV arise in an accretion disc illuminated by the central source. If the line originates in a disc, its line profile should be broadened and shifted by the effects of gravitational redshift and the Doppler effect. The detailed line shape is sensitive to the inclination of the disc, the distribution of line-emitting material, and the metric (e.g. Fabian et al. 1989; Laor 1991).

The poor spectral resolution of X-ray spectrometers before *ASCA* gave only a hint of broad iron K emission in active galaxies (Nandra & Pounds 1994). The CCD spectrometers on board *ASCA* have an energy resolution ∼10 times better than that of proportional counters and enable us to measure the line profile. The detection of broad iron K lines from cold matter in the Seyfert 1 galaxies IC 4329A and NGC 5548 was reported by Mushotzky et al. (1995). Subsequently, a well-resolved line in MCG − 6-30-15,

skewed to lower energy, has been presented by Tanaka et al. (1995).

IRAS 18325 − 5926 is an *IRAS*-selected Seyfert 2 galaxy (de Grijp et al. 1985) at a redshift $z = 0.0198$ (Iwasawa et al. 1995). An X-ray source H 1829 − 591 was identified with this galaxy by Ward et al. (1988). Optical spectroscopy indicates a large Balmer decrement (Hα/Hβ $\simeq 10$), implying that the emission-line region is reddened by $A_v \approx 3.5$ mag. The Balmer lines have weak wings (Carter 1984; Iwasawa et al. 1995), with the Hα wing being broad (*FWHM* = 3400 km s^{-1}), suggesting the presence of an obscured Seyfert 1 nucleus. This was verified by the detection of a variable X-ray source in the *Ginga* observation (Iwasawa et al. 1995).

The *Ginga* X-ray spectrum shows a relatively steep power-law continuum of photon index $\Gamma \sim 2.2$, with moderate X-ray absorption of $N_H \sim 1 \times 10^{22}$ cm^{-2}, consistent with the optical reddening. During the *Ginga* observation, the source exhibited rapid X-ray variability on time-scales from 10^4 s down to a few times 10^3 s, and the absorption-corrected average X-ray luminosity in the 2–10 keV band was $L_X = 5 \times 10^{43}$ erg s^{-1} (we use $H_0 = 50$ km s^{-1} Mpc^{-1} throughout this paper). Fits to the *Ginga* spectrum indicate that the Fe K feature is broad, and no significant reflection hump is present.

We report in this paper the soft X-ray properties and evidence for a broad, strong iron K emission feature in the *ASCA* spectrum of IRAS 18325 − 5926.

2 OBSERVATIONS AND DATA REDUCTION

IRAS 18325 − 5926 was observed with *ASCA* on 1993 September 11–12. A summary of *ASCA* and its performance appears in Tanaka, Inoue & Holt (1994). The SIS detectors (S0 and S1) were operated in 4CCD mode. The data reduction was done using the standard *ASCA* software FTOOLS and XSELECT. About 32 ks of useful data from both GIS (S2 and S3) were obtained. The reflection of sunlight from the bright Earth contaminated the SIS data below 1 keV. We therefore discarded data when the line of sight fell below 25° from the bright rim of the Earth when studying the soft X-ray spectrum. The hot/flickering pixels of the CCD detectors were removed. While useful data of about 36 ks were obtained from S0, some parts of the S1 data are of very low count rate, due to the source lying in the dead region between the CCD chips as the pointing attitude of the telescope fluctuated. The S1 data thus obtained were 20 ks. The X-ray image is point-like as viewed by the *ASCA* XRT. Source data were taken from a circular region with a radius of 4 arcmin for the SIS and a radius of 5 arcmin for the GIS, respectively.

IRAS 18325 − 5926 [Galactic coordinates $(l, b) = (335.^\circ98, -21.^\circ34)$] lies in a relatively bright part of the soft X-ray sky as seen in the M-band (0.4–1 keV) maps from the Wisconsin sky survey and the *HEAO-1* A2 LED survey (McCammon & Sanders 1990) due to diffuse Galactic thermal emission. In agreement with these results we find excess soft X-rays below 2 keV taken from an off-source region in the detector field of view, compared with the mean background spectrum derived from a set of blank-sky observations (e.g. Gendreau et al. 1995). The local sky is brighter by a factor of ~ 2 in the 0.4–2 keV band than the mean background. We thus utilize local background for the spectral

analysis. The average count rates corrected for the background are 0.26 (S0), 0.20 (S1), 0.25 (S2) and 0.26 (S3) count s^{-1}.

ROSAT PSPC (Trümper 1983; Pfeffermann et al. 1987) observations were made of IRAS 18325 − 5926 on 1992 October 12 (RP 701017; 9312-s exposure) and 1993 September 11–12 (RP 701415; 11864-s exposure). During RP 701017, IRAS 18325 − 5926 was 35.5 arcmin off-axis in the field of view and was partially shadowed by one of the ribs that forms part of the PSPC entrance window support structure. During RP 701415, IRAS 18325 − 5926 was on-axis, and this observation partially overlapped in time with the *ASCA* observation (see Fig. 1). The average observed count rates after background subtraction (correcting to the centre of the PSPC field of view for RP 701017) were 0.24 count s^{-1} for RP 701017 and 0.18 count s^{-1} for RP 701415. The PSPC radial profile does not show any significant evidence for spatial extent. Reduction and analysis of the PSPC image data was performed with the Starlink ASTERIX X-ray data processing system. We have extracted source counts for IRAS 18325 − 5926 from a circular source cell chosen to be large enough to ensure that all of the source counts are included. Background counts were subtracted from the source cell using a large nearby circular source-free background cell. Systematic errors of 2 per cent were added in quadrature to the data point rms errors, to account for residual uncertainties in the spectral calibration of the PSPC. We have used the 1993 January response matrix (MPE No. 36) for the spectral fitting (this is the recommended matrix according to the PSPC team). This matrix corrects for the systematic deficit of photons near the carbon edge of the PSPC detector that was present in earlier matrices (cf. Turner, George & Mushotzky 1993). Errors quoted for quantities are at the 90 per cent confidence level.

3 RESULTS

3.1 Broad-band spectrum and time variability

The broad-band spectra (0.4–10 keV) of IRAS 18325 − 5926 in S0 and S1 were fitted with an absorbed power-law model (Fig. 2). There is weak surplus emission below 1 keV, which is also seen in S2 and S3 spectra. Similar results are seen in narrow-emission-line galaxies (Mulchaey et al. 1993) and in NGC 4151 (Weaver et al. 1994), and have been interpreted as either emission from an extended component or electron scattering of the central source by an extended electron cloud. We attempt to understand the broad-band nature of the energy spectrum and to address the origin of the excess of soft X-ray emission by spectral analysis combined with time variability analysis. The following investigations were made using the SIS data, because of their better sensitivity to soft X-rays than GIS.

The *ASCA* and second *ROSAT* observations were partially simultaneous, with the *ROSAT* observation leading the *ASCA* one by 6 h. There was an overlapping observing run of 14 h by both satellites. During these observations, the X-ray flux of the source changed on a typical time-scale of 10^4 s (Fig. 1), which confirms the short variability in this source observed by *Ginga* (Iwasawa et al. 1995). The variability of the X-ray flux above 1 keV is obvious, but below
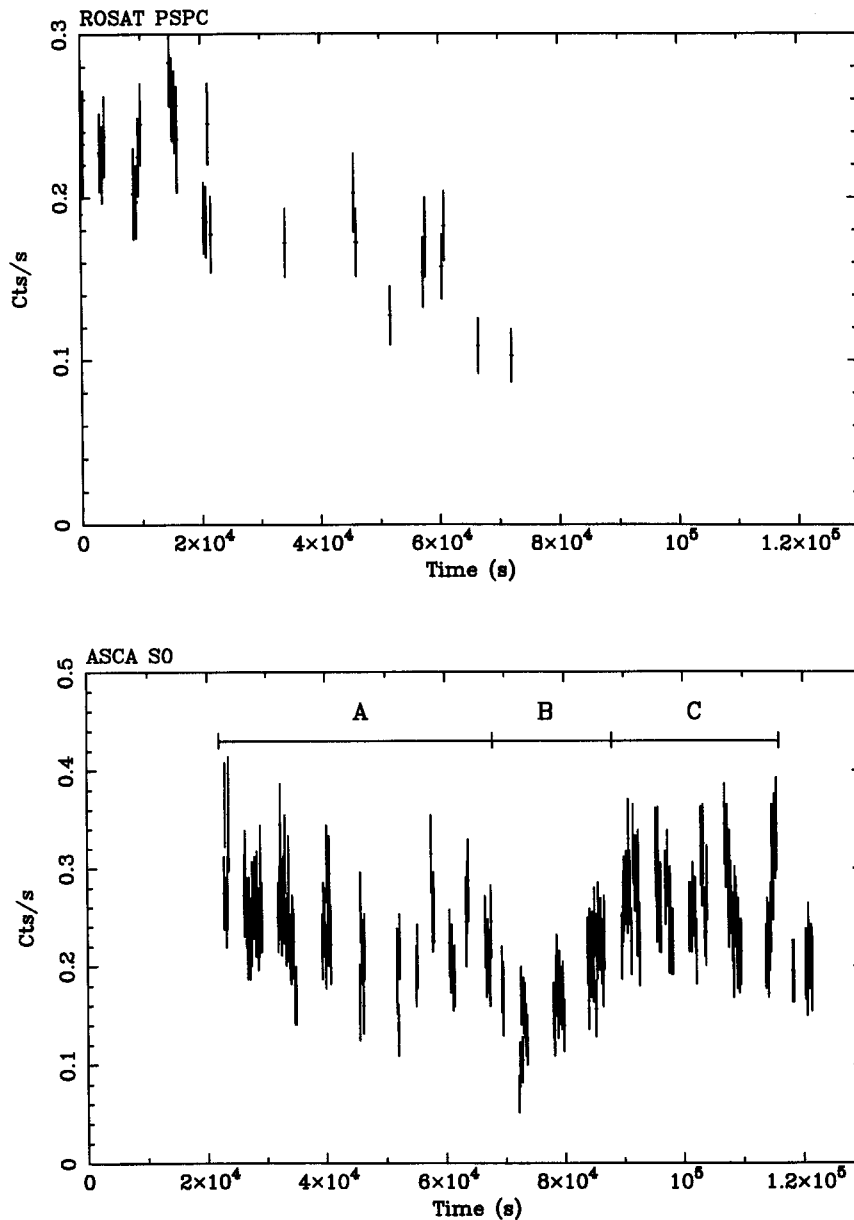
Figure 1. The X-ray light curves of IRAS 18325 – 5926 from the second *ROSAT* (RP 701415) and the *ASCA* observations with an epoch 05:52, 1993 September 11. Clear flux changes on a time-scale of $\sim 10^4$ s were observed. The fastest change of flux was detected by *ASCA* between 1.06×10^5 and 1.15×10^5 s, where the observed count rate changed by a factor of 2 in 2000–3000 s.

1 keV it is unclear because of its relatively low count rate. We divided the *ASCA* observing run into three time bins (A, B and C) as shown in Fig. 1, which represent periods of medium, low and high count rate, respectively. Comparing their background-subtracted count rates in the two energy bands (0.4–1 and 1–10 keV; Fig. 3), the change of soft X-rays seems smaller than that of the hard X-rays. Fig. 4(a) shows *ASCA* SIS spectra taken in B and C, and the ratio of C to B. Above 1 keV, the ratio is consistent with an average value ~ 1.4. However, it decreases toward unity below 1 keV. The hypothesis of a constant ratio is ruled out at the ~ 90 per cent confidence level. This trend was also seen in a similar plot from the 1–26 000 and 26 000–75 000 s *ROSAT* data (Fig. 4b). The manner of variability suggests the

presence of a time invariant or at least a less-variable component in the soft X-ray band, and we identify it with the soft excess emission in the energy spectrum. It should be of a count rate $\sim 6 \times 10^{-3}$ count s^{-1} in the SIS spectrum, and take ~ 60 per cent of counts below the 1-keV band during B. The variability argues against the possibilities for the soft excess such as X-rays escaping from a patchy line-of-sight absorber, or excess emission intrinsic to the central source.
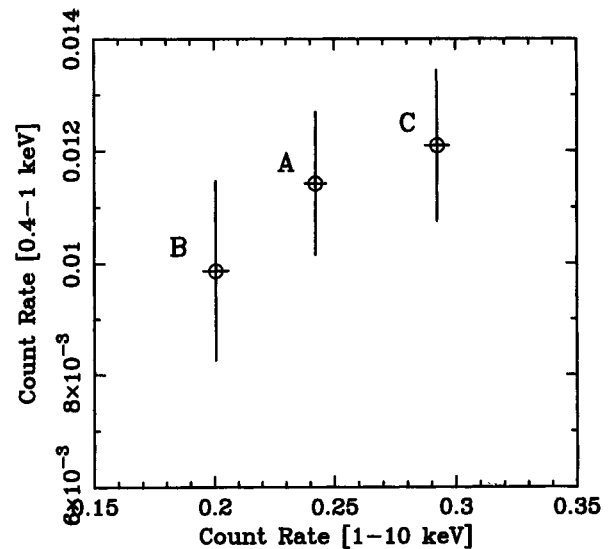
Next, we fit the energy spectra by a Raymond–Smith thermal spectrum or a power law in addition to the primary power-law component. Since the broad Fe K feature around 6 keV (see next section) affects the determination of the power-law slope, a broad Gaussian model for the Fe K line
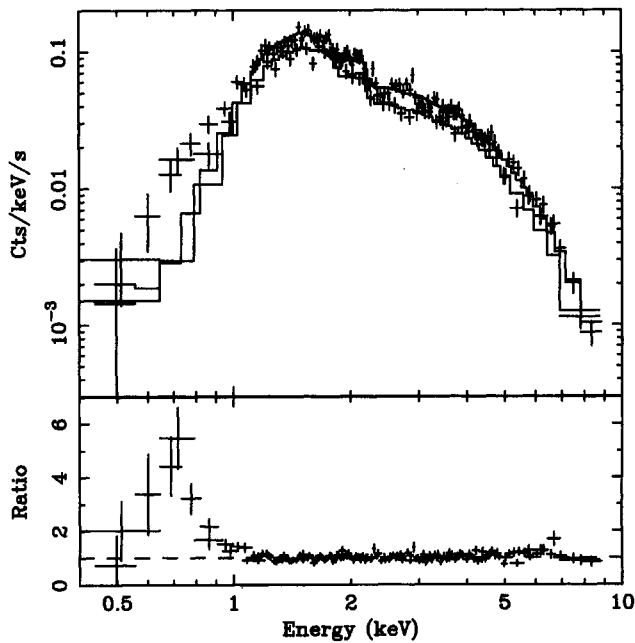
Figure 2. The *ASCA* 0.4–10 keV spectra of IRAS 18325 − 5926 from *ASCA* S0 and S1 after the nearby background has been subtracted. The solid line indicates the 1–10 keV best-fitting absorbed power-law model, $\Gamma = 2.2$ and $N_H = 1.2 \times 10^{22}$ cm^{-2}. The lower panel is a plot of ratios of data and the model spectrum. Weak excess emission above the model can be seen below 1 keV.

Figure 3. Plot of count rates in the 1–10 and 0.4–1 keV bands obtained from the background-subtracted data during A, B and C periods in the *ASCA* light curve in Fig. 1.

was included in the fit. The *ASCA* SIS data and the PSPC data in the second *ROSAT* observation were jointly fitted. The first *ROSAT* data set was excluded in this spectral analysis because of its worse quality due to the off-axis position; it is used only for X-ray flux derivation. The accuracy of calibration between the two satellites has been checked using the data from the period 26 000–75 000 s (Fig. 1), when data were simultaneously taken by both satellites. *ROSAT* calibration uncertainties are discussed in appendix A of Brinkmann et al. (1994), and appendices A and B of Fiore et al. (1994). Calibration discrepancies between *ASCA* and *ROSAT* data are suspected in the simultaneous NGC 5548 data reported on by Fabian et al. (1994) (although the nature of the discrepancies is not discussed in this reference). Fewer counts were collected from IRAS 18325 − 5926 than NGC 5548, and hence spectral model parameters for IRAS 18325 − 5926 cannot be constrained with the same high precision as they can be for NGC 5548. Calibration uncertainties appear to be smaller than statistical uncertainties for this object. The *ROSAT* data do, however, have about a 6 per cent larger normalization than the *ASCA* data. This was taken into account for the analysis below, and derived fluxes and luminosities are based on the *ASCA* data. A summary of the fits are shown in Table 1.

The photon index and absorption column density of the primary power law are $\Gamma = 2.12 \pm 0.08$ and $N_H = (1.12 \pm 0.08) \times 10^{22}$ cm^{-2}. A thermal spectrum of $kT = 0.35 \pm 0.06$ keV and cosmic abundance with a Galactic column density ($N_H = 5 \times 10^{20}$ cm^{-2}) is also a good description of the soft excess component (Table 1). The fraction of the thermal component in the 0.4–1 keV band (65 ± 20 per

cent in photons) is consistent with the result from the above study of X-ray colour versus intensity changes. Fits to the time-resolved spectra in A, B and C give a very similar normalization of the thermal component. This supports the extended nature of the soft emission from the unobscured region well outside the nucleus, and hence its lack of variability. The luminosity of the thermal spectrum is 1.1×10^{41} erg s^{-1} in the 0.5–2 keV band. This is about one order of magnitude greater than that of extended thermal emission observed in nearby spiral galaxies (e.g. Fabbiano, Kim & Trinchieri 1992; Makishima et al. 1994), and is similar to the X-ray halo in elliptical galaxies (Awaki et al. 1994; Loewenstein et al. 1994). Ward et al. (1988) reported that the optical morphology of the host galaxy (Fairall 49) is S0-type, unlike most ordinary Seyfert nuclei which are located in late-type spirals. Thus the large X-ray luminosity of the thermal X-ray emission may not be peculiar. However, the *ROSAT* PSPC image showed that the extent of the X-ray source is not much beyond its spatial resolution $FWHM \simeq 25$ arcsec, which corresponds to a size of 14 kpc at the galaxy redshift. This should be comparable to the extent of any X-ray-emitting gas. Note that the nuclear source dominates the total X-ray emission, so that weak extended emission could not be resolved by *ROSAT*.

In the power-law model, the photon index of the soft power law is assumed to be identical to that of the major component, which we suppose to be due to electron scattering of X-rays from the central source. When the absorption is just the Galactic one, the scattering fraction is about 2.5 per cent, but the fit is worse than the thermal model (Table 1). The fit is improved by extra absorption of $N_H \sim 2 \times 10^{21}$ cm^{-2}, smaller than the optical reddening, $A_V = 3.5$ corresponding to $N_H = 7 \times 10^{21}$ cm^{-2} at the Galactic dust-to-gas ratio. However, the derived scattering fraction is 13–17 per cent, the results being sensitive to the assumed power-law slope. This range is unusually high, comparing with that (one–a few per cent: Koyama 1992; Mulchaey et al. 1992) observed in other Seyfert 2 galaxies, and requires a large
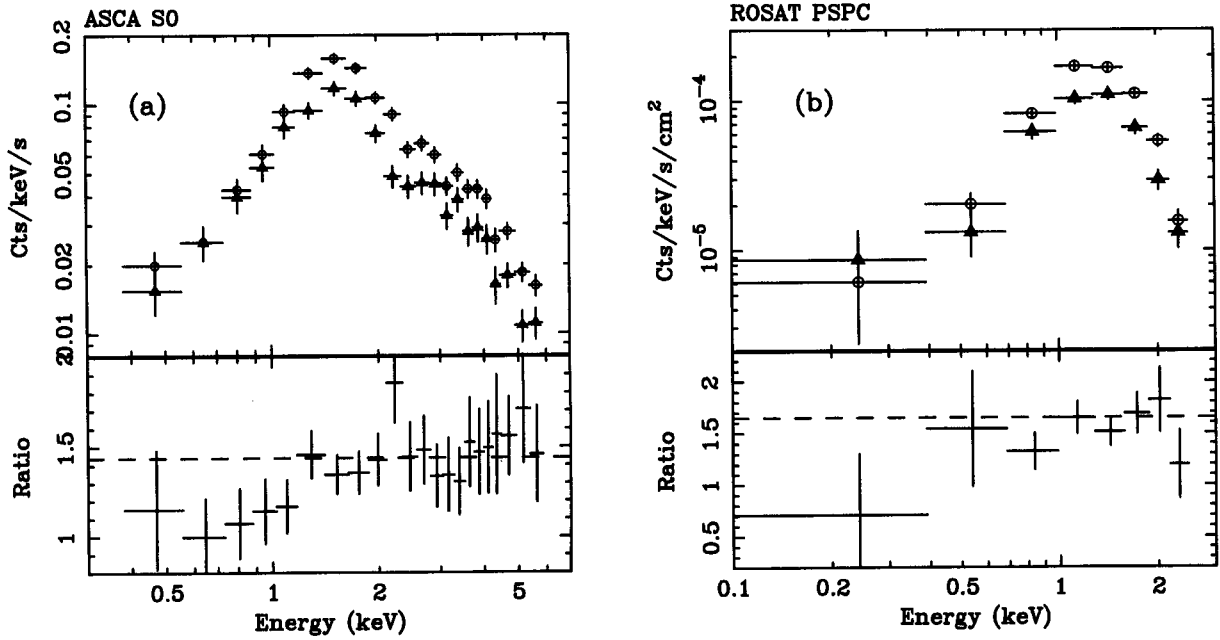
Figure 4. (a) *ASCA* S0 energy spectra taken during B (faint period; filled triangles) and C (bright period; open circles) are shown on the upper panel. The lower panel shows their count rate ratios of C relative to B. The weighted mean value of the ratio above 1 keV is 1.44, which is indicated by a dashed line, while the ratio drops toward unity below 1 keV. This plot demonstrates the spectral variability. (b) Similar plot for the first 26 000 s (open circles) and the 26 000–75 000 s (triangles) of *ROSAT* data.

Table 1. Spectral fits to *ASCA* SIS (S0, S1) and *ROSAT* PSPC (RP701415) spectra. PL_1 is the primary power-law component, and PL_2 is the secondary one. RS is the Raymond–Smith thermal emission spectrum. (G) means the Galactic absorption deduced from the $E(B - V) = 0.09$, assuming the standard dust-to-gas ratio. (I) means the absorption intrinsic to the secondary power law. N_2/N_1 is the normalization ratio of PL_2 and PL_1, which implies a scattering fraction.

Model	Primary power-law	Secondary component	χ^2/dof
(1) PL_1	$\Gamma_1 = 1.98 \pm 0.05$	—	451.9/383
	$N_{H1} = (0.95 \pm 0.05) \times 10^{22} cm^{-2}$	—	
(2) PL_1 + RS (G)	$\Gamma_1 = 2.12 \pm 0.08$	$kT = 0.35 \pm 0.06$ keV	376.7/379
	$N_{H1} = (1.12 \pm 0.08) \times 10^{22} cm^{-2}$	$Z = 1Z_\odot$	
		$N_{H2} = 5 \times 10^{20} cm^{-2}$	
(3) PL_1 + PL_2 (G)	$\Gamma_1 = 2.07 \pm 0.07$	$\Gamma_2 = \Gamma_1$	407.3/380
	$N_{H1} = (1.13 \pm 0.08) \times 10^{22} cm^{-2}$	$N_{H2} = 5 \times 10^{21} cm^{-2}$	
	$N_2/N_1 = 0.024 \pm 0.01$		
(4) PL_1 + PL_2 (I)	$\Gamma_1 = 2.30 \pm 0.15$	$\Gamma_2 = \Gamma_1$	372.7/379
(4) PL_1 + PL_2 (I)	$\Gamma_1 = 2.30 \pm 0.15$	$\Gamma_2 = \Gamma_1$	372.7/379
	$N_{H1} = (1.65 \pm 0.30) \times 10^{22} cm^{-2}$	$N_{H2} = (4.3 \pm 1.5) \times 10^{21} cm^{-2}$	
	$N_2/N_1 = 0.13^{+0.07}_{-0.05}$ (ASCA); $0.17^{+0.11}_{-0.08}$ (ROSAT)		

optical depth of ionized gas. This is possible only in a region very close to the central source, which is well inside the X-ray-absorbing matter. If such a high fraction of the central source is scattered to us, polarization arising from electron scattering, and scattered broad emission lines, would be observed in the optical band. Although a high optical polari-zation ($P = 5.7$ per cent at the V band; Brindle et al. 1990) and weak broad wings on the Balmer lines have been observed (Carter 1984; Iwasawa et al. 1995), a dust screen and its extinction are favoured for their origin, as discussed in Iwasawa et al. (1995). Thus a scattered power-law compo-nent is unlikely.

Table 2. Oberved fluxes and absorption corrected luminosities. *: Absorption-corrected luminosities for the primary component of power-law averaged during each observation.

| Flux (erg cm^{-2} s^{-1})	0.5–2 keV	2–10 keV
ROSAT 1st	2.8×10^{-12}	—
ROSAT 2nd	2.4×10^{-12}	—
ASCA	1.6×10^{-12}	8.4×10^{-12}
L_X^* (erg s^{-1})	0.5–2 keV	2–10 keV
ROSAT 1st	2.7×10^{43}	—
ROSAT 2nd	2.3×10^{43}	—
ASCA	1.5×10^{43}	1.6×10^{43}

An interesting possibility for the soft X-ray spectral complexity is a non-solar-abundance absorber. A cold absorber with a supersolar abundance of iron ($\sim 10\,Z_\odot$), as suggested for the accretion disc (Section 4), imposes a deep iron L absorption edge on the *ASCA* spectrum. This possibility is not supported by the different soft and hard X-ray variability behaviour.

The average observed flux in the 2–10 keV band, $f_X = 0.9 \times 10^{-11}$ erg cm^{-2} s^{-1}, from the *ASCA* data is a factor of 3–4 lower than that during the *Ginga* observation in 1989. Correcting for intrinsic absorption, the 2–10 keV X-ray luminosity is $L_X = 1.6 \times 10^{43}$ erg s^{-1}. In the 0.5–2 keV band, the observing fluxes during the first and second *ROSAT* and the *ASCA* observations are 2.8×10^{-12}, 2.4×10^{-12} and 2.0×10^{-12} erg cm^{-2} s^{-1}, respectively. The fluxes and the absorption-corrected luminosities for each component in each observation are given in Table 2.

3.2 Broad Fe K line feature

In order to avoid unnecessary complexity in the spectral fitting from the external soft component, we restrict our fitting to energies above 1.5 keV for detailed spectral analysis of the Fe K line region. We also utilize a single absorbed power law as the underlying continuum in this analysis. There should be little effect of reflection on the continuum shape in the *ASCA* band, because of the lack of either the hard continuum tail or an iron K absorption edge in the *Ginga* spectrum of this object (Iwasawa et al. 1995; Smith & Done 1995).

As seen in Fig. 5, the broad Fe K feature around 6 keV is readily apparent. Modelling of the emission-line feature by a narrow Gaussian, with dispersion $\sigma = 0.05$ keV, results in poor residuals, even if an absorption edge due to Fe K is included (see Table 3). As suggested by the *Ginga* spectrum (Iwasawa et al. 1995), a good fit to the data requires that the line be broad. If a single broad Gaussian is fitted to the Fe K line, the fit is significantly improved ($\Delta\chi^2 = 28.2$), with the broadening of the line being significant at about the 99 per cent confidence level. The line energy, dispersion, and equivalent width are $E = 6.1^{+0.2}_{-0.3}$ keV, $\sigma = 0.85^{+0.5}_{-0.3}$ keV, and $EW = 580^{+400}_{-250}$ eV, respectively. Line energies quoted here and hereafter are as observed unless explicitly stated other-
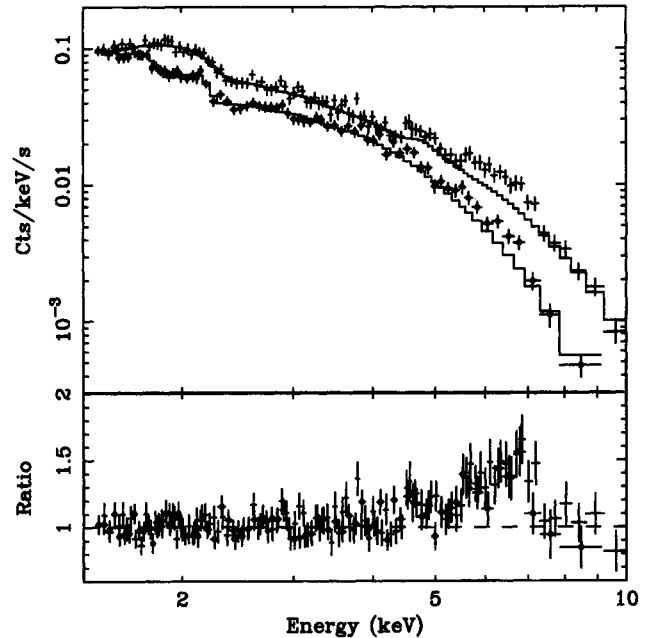
Figure 5. *ASCA* SIS and GIS spectra in the 1.5–10 keV band. Upper panel: SIS (filled circles) and GIS (crosses) data, and the best-fitting power-law continuum (solid lines). Plot is created setting normalization of disc-line model to zero after fitting by the Fabian89-Cold (2) model in Table 3. Lower panel: ratio plot of data to the continuum model. A very broad emission feature is clearly visible from 4 to 7 keV. The energy resolution around 6 keV is FWHM ≈ 130 eV in the SIS and ≈ 460 eV in the GIS.

wise: a 6.40-keV iron K line should be redshifted to 6.27 keV in this object.

The line is peaked at around 6.8 keV, and skewed toward low energy. Modelling with two Gaussians gives a narrow core at 6.76 ± 0.06 keV and a broad component around $5.8^{+0.3}_{-0.4}$ keV with $\sigma = 0.95^{+0.5}_{-0.3}$ keV (Table 3). Significant peaks are also present at 5.6 and 4.6 keV on the broad feature. There is an instrumental structure around 4.6 keV only in the GIS spectrum due to the Xe edge from the counter filling gas, which might make the feature unreliable. However, detection of the same peak in the SIS spectrum supports its presence. Such a very broad line with FWZI up to the half velocity of light could only be possible for the innermost part of the accretion disc (Fabian et al. 1995). The energy of the blue peak is significantly higher than that in MCG -6-30-15, where the *ASCA* spectrum shows the blue peak at 6.4 keV (Tanaka et al. 1995). Such an extremely broad and skewed line is interpreted as having been affected by Doppler broadening and gravitational shift at the innermost part of the accretion disc around the black hole (e.g. Fabian et al. 1989; Chen, Halpern & Filippenko 1989; Laor 1991).

We fit the model of the relativistic line by Fabian et al. (1989) for the Schwarzschild black hole. The initial line energy, E, inclination of the disc, i, inner and outer radii, R_{in} and R_{out}, and the index of the emissivity law ($\propto R^{-\alpha}$), α, are the free parameters. It is hard to assess the initial line energy directly from the present data, since the line shape largely depends on the inclination of the disc, and the radius where the line originates. At first we assumed the initial energy of a cold iron line, which should be 6.4 keV in the

Table 3. Spectral fits to the *ASCA* SIS and GIS data in the 1.5–10 keV band using an absorbed power law and (a) a Gaussian or two Gaussians, and (b) a disc-line model by Fabian et al. (1989; Fabian89) for a Schwarzschild black hole and by Laor (1991; Laor91) for a rotating Kerr black hole. See the text for a detailed description of each parameter. Line energies are indicated in the observed frame. 'Cold' and 'He-like' mean that the initial rest-energies are 6.4 and 6.7 keV, respectively. 'Cold (1)' and 'Cold (2)' are for the cases of local minima corresponding to the red horn at 5.6 and 4.6 keV, respectively.

(a) Gaussian line

Line Model	Power-law			Gaussian		χ^2/dof
	Γ	$N_{\rm H}$	E	σ	EW	
		$10^{22}{\rm cm}^{-2}$	keV	keV	keV	
NL	2.17 ± 0.05	1.12 ± 0.10	6.72 ± 0.06	0.05	0.17 ± 0.05	547.3/532
BL	2.32 ± 0.06	1.32 ± 0.10	$6.1^{+0.2}_{-0.3}$	$0.85^{+0.5}_{-0.3}$	$0.58^{+0.40}_{-0.25}$	519.1/531
BL + NL	2.32 ± 0.08	1.32 ± 0.10	$5.8^{+0.3}_{-0.4}$	$0.95^{+0.5}_{-0.3}$	$0.65^{+0.5}_{-0.3}$	510.6/527
			6.76 ± 0.06	$0.02^{+0.35}_{-0.02}$	0.14 ± 0.05	

(b) Disc-line

| Line Model	Power-law		E	α	$R_{\rm in}$	$R_{\rm out}$	i	EW	χ^2/dof
	Γ	$N_{\rm H}$							
		$10^{22}{\rm cm}^{-2}$	keV		$R_{\rm S}$	$R_{\rm S}$	°	keV	
Fabian89									
Cold (1)	2.26 ± 0.14	1.30 ± 0.15	6.27	1	3	40^{+35}_{-14}	51^{+22}_{-8}	0.57 ± 0.23	512.6/531
Cold (2)	2.27 ± 0.15	1.31 ± 0.20	6.27	1	3	7^{+2}_{-1}	42 ± 3	0.81 ± 0.32	510.4/531
He-like	2.30 ± 0.14	1.31 ± 0.20	6.57	1	3	5.5 ± 1.5	36 ± 3	0.84 ± 0.34	510.1/531
Laor91									
Cold	2.30 ± 0.15	1.23 ± 0.15	6.27	2	0.63	6.5 ± 3.5	44^{+5}_{-3}	1.07 ± 0.41	509.1/531
He-like	2.30 ± 0.15	1.31 ± 0.20	6.57	2	$1.5^{+0.4}_{-0.8}$	$5.5^{+1.5}_{-1.0}$	38^{+3}_{-2}	$0.92^{+0.36}_{-0.28}$	507.1/530

rest-frame. This model gives a good fit, compared with the broad Gaussian model (see Table 3). In this model, the line profile is essentially double-horned, and two different choices of the red horn of either a peak at 5.6 keV or one at 4.6 keV are allowed. The fit therefore falls into two local minima corresponding to the two cases. The value of $R_{\rm in}$ is not well constrained, and we assume $R_{\rm in} = 3\,R_{\rm S}$, where $R_{\rm S}$ is the Schwarzschild radius, and $3\,R_{\rm S}$ is the minimum value for a bound orbit in the Schwarzschild geometry.

In the former case [Cold (1) in Table 3], an inclination of $i \sim 50°$, $R_{\rm out} \sim 46\,R_{\rm S}$, and equivalent width, $EW = 570 \pm 230$ eV, similar to that of the Gaussian model are obtained, for $\alpha = 2$. A very steep emissivity law of α larger than 4 is ruled out. As shown in Fig. 6, the line is shifted both redward and blueward from the initial energy and forms an asymmetric profile with the relativistic effect boosting the blue horn at such a large inclination. Fitting for the latter case [Cold (2) in Table 3] gives a slightly better fit ($\Delta\chi^2 = 2$), with a larger equivalent width, $EW = 800 \pm 340$ keV. We find a smaller $R_{\rm out} \sim 7\,R_{\rm S}$, which implies that the line-emitting region must

be closer to the central source where the redshift is pronounced. The inclination is still large, with $i = 42° \pm 3°$.

In the Kerr metric, which is appropriate for a spinning black hole, a smaller innermost radius of the disc is allowed than for a Schwarzschild black hole. We fitted the emission-line model of the Kerr black hole by Laor (1991), which is, in most cases, characterized by a blueshifted steep line-peak and a broad red wing. This model also describes the broad profile from 4 to 7 keV well. The best-fitting values of the parameters are $R_{\rm in} = 0.63\,R_{\rm S}$ (minimum value), $R_{\rm out} = 6.5^{+10}_{-3.5}\,R_{\rm S}$, $i = 44°^{+5°}_{-3°}$, $\alpha = 2^{+2}_{-3}$, and $EW = 1.07 \pm 0.38$ keV.

We can rule out the possibility of a deep iron K absorption edge explaining the broad spectral feature. The line emission declines sharply around 7 keV, which is close to the threshold energy of the K-shell absorption edge of neutral iron. In this case, however, the observed line peak at a rest energy of 6.9 keV which is indicative of hydrogen-like iron, is not consistent with the ionization state implied by the edge energy. Even if the edge is included in the fit, the broad profile still remains.

© 1996 RAS, MNRAS **279**, 837–846
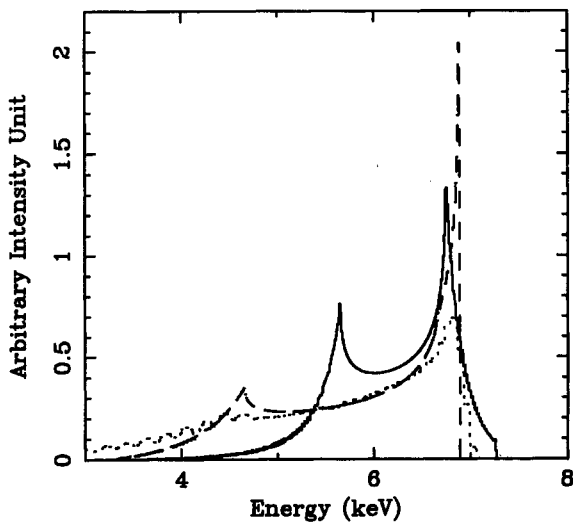
Figure 6. Calculated line profiles fitted to the observed line for a Schwarzschild black hole (Fabian et al. 1989) and a Kerr black hole (Laor 1991). Initial rest energy of the line, 6.4 keV, is assumed, and the profiles correspond to Fabian89-Cold(1): solid line, Fabian89-Cold(2): dashed line, and Laor91-Cold: dotted line in Table 3. Note that these profiles are *not* folded through the detector response.

The equivalent width is much higher than the prediction of reflection from a cold disc with solar composition and abundance (George & Fabian 1991). The observed inclination of the disc reduces the equivalent width further. This suggests a supersolar abundance of iron. The lack of reflection signatures in the *Ginga* spectrum is consistent with a large inclination and high metal abundance. These problems will be discussed later.

As discussed later, a highly ionized disc is a possible solution for the large equivalent width (Matt et al. 1993; Życki & Czerny 1994). Even though the actual line shape from the ionized disc might be considerably complicated (Matt et al. 1993), we approximate it by the disc-line model, just shifting the initial rest-energy to 6.7 keV appropriate for emission line from He-like iron (Fe xxv). In this case, a substantial fraction of the line emission must be shifted to the red mainly by gravitational redshift. Fits by disc-line models both for Schwarzschild and Kerr metrics give similar parameters: $R_{out} \simeq 5.5 R_S$, $i \simeq 37°$, $EW = 840 \pm 340$ keV, with the qualities of fit comparable to the cold-line models (Table 3). The EW tend to be larger than in the case of the cold line. These fits for the line are shown in Table 3. Note that, in any fits, residuals from the disc-line model show significant line-like features across the broad feature at either 4.6 or 5.6 keV with equivalent widths of 30–60 eV depending on the particular disc-line model fit.

4   DISCUSSION

The Fe K emission line in the X-ray spectra of Seyfert 1 nuclei has been well explained in terms of reflection from cold material (George & Fabian 1991). The mean line energy of $E = 6.37 \pm 0.06$ keV and equivalent width $EW = 140 \pm 20$ eV of the *Ginga* sample (Nandra & Pounds 1994) are in good agreement with the cold reflection model

which can also account for the high-energy hump above 10 keV commonly seen in Seyfert 1 spectra (Guilbert & Rees 1988; Lightman & White 1988; George & Fabian 1991).

However, the iron K line features in active galaxies are actually broad, even though the *Ginga* spectra were fitted with a narrow line. *ASCA* has resolved broadening of the line in several objects (Fabian et al. 1995, and references therein). A long *ASCA* observation of MCG – 6-30-15 (Tanaka et al. 1995) showed a considerable fraction of the line emission shifted to lower energy. The large shift of the line ($\Delta E \sim 1$–1.5 keV) and its shape are possible only when the line originates in the inner part of an accretion disc around a massive black hole where the gravitational and Doppler shift are pronounced, as discused in Fabian et al. (1995) and Mushotzky et al. (1995). Fits to the broad line features with the disc-line models provide the inclination of the disc, and most of them show it to be around 30° (Fabian et al. 1995). This may be a selection effect, since strong emission with broadening appropriate to the *ASCA* energy resolution favours such inclination. Also, the blue horn is peaked at 6.4 keV in such an inclination, which could be a reason why the line energies in the Seyfert 1 sample are close to 6.4 keV when a narrow line was fitted to *Ginga* data of poorer resolution (Nandra & Pounds 1994).

The *Ginga* observation of IRAS 18325 – 5926 showed that it was roughly similar to Seyfert 1 galaxies, but the spectrum had a steeper continuum slope $\Gamma \simeq 2.2$ without a significant reflection hump and probably had a broad Fe K emission line (Iwasawa et al. 1995). Present *ASCA* observations resolve a very broad feature from 4 to 7 keV, and show that the line shape is consistent with emission produced in the accretion disc. The line is peaked around a rest-energy of 6.9 keV, significantly higher than the 6.4 keV seen in most of the broad Fe K lines resolved so far. If the line originates in cold matter (the initial energy should be 6.4 keV), the shifts of the line are toward both red and blue, in contrast to the others which are mainly shifted to red. Consequently, the cold disc-line model fit gives an intermediate inclination, $i \simeq 40°$–50°, considerably larger than $i \sim 30°$ in other objects (e.g. Mushotzky et al. 1995; Tanaka et al. 1995). This could also be compatible with the Seyfert 2 classification, if it depends on the orientation of the putative obscuring torus, since it is close to the critical angle for occulting the central source.

Here we note that R_{out} is small in most disc-line fits. The outer radius of the line-emitting region is probably larger than the half-power radius of the disc, which is about $10 R_S$ for a Schwarzschild geometry in the Newtonian approximation (Shakura & Sunyaev 1973). The 'Cold (1)' model is then preferred. If a small value of R_{out} is true, then the Kerr geometry is relevant, since the half-power radius is smaller than in the Schwarzschild geometry. It also implies that the X-rays are produced very close to the surface of the accretion disc rather than, for example, in a 'quasi-jet' forming region at the symmetrical axis much higher above the disc.

Another remarkable property of the line is its large equivalent width ($EW = 500$–1000 eV). The cold reflection model for solar abundance (George & Fabian 1991) predicts at most $EW = 150$ eV from fluorescent iron emission. Large equivalent widths have been observed by *ASCA* in several Seyfert 1 galaxies with broad lines: $EW = 250$–400 eV in MCG – 6-30-15 (Tanaka et al. 1995), $EW = 550 \pm 250$ eV in

Mrk 1040 (Reynolds, Fabian & Inoue 1995), and $EW \simeq 600$ eV in Fairall 9 (Otani et al. 1995, in preparation). A possible option for that is the supersolar abundance of iron relative to lighter elements which also suppresses the reflection hump. Evidence for supersolar abundance in active galaxies has been provided by various observations (e.g. Reynolds et al. 1995). This abundance effect on the EW of iron line is discussed in several papers (George & Fabian 1991; Matt, Perola & Piro 1991; Życki & Czerny 1994; Reynolds et al. 1995). If iron in the accretion disc has an abundance of 10 times the solar value and lighter elements remain at the cosmic values of Anders & Grevesse (1989), an $EW \sim 600$ eV can be expected for reflection from a cold disc from fig. 4 in Reynolds et al. (1995). To account for the lower range of the EW, at least three times the solar abundance of iron is required, unless oxygen is ·not significantly deficient. When the line originates in the disc very close to the central hole, Doppler boosting at the blue side of the disc and the light bending effect could maintain the large EW at high inclination, and hence weaken the inclination dependence of EW (Matt et al. 1992). The small implied value of R_{out} ($\approx 6\,R_s$) suggests that most of the line emission is produced at the innermost part of the accretion disc. Therefore the relativistic effect could assist the large equivalent width of IRAS 18325 − 5926, since at $i = 40°$–$50°$, the equivalent width drops by only ~10 per cent from the value for the face-on disc (Matt et al. 1992). A relative deficiency of lighter elements also leads to a further increase in EW of the iron line, since they, in particular oxygen, are the primary absorber of the iron fluorescent line photons. The observed large EW is thus explicable by these abundance effects apart from iron L absorption.

We note that the anisotropy of the radiation in the reflection scenario (Ghisellini et al. 1991) is unlikely to be important at the energy of the iron line, if the primary continuum is due to a thermal plasma (or a non-thermal one with low mean electron energy). CGRO data from *OSSE* indicate that thermal Comptonization is a plausible source of emission for many Seyfert galaxies (Zdziarski et al. 1994). Anisotropy is most important in the first scattering of the input soft photons, which are presumably of energy less than 0.1 keV. The energy of the scattered photons are at most a few keV (see simulations in Haardt 1993), too low to boost the equivalent width of the iron line.

An alternative possibility for the large EW is an ionized disc. If the matter in the disc is highly ionized, the opacity for the line photons escaping from the disc becomes smaller and the fluorescence yield increases as a function of the ionization stage; in particular, it reaches the maximum at He-like iron, Fe xxv (Matt et al. 1993; Życki & Czerny 1994). These effects combined together could increase the EW by a factor of two over that from a cold disc. It also makes the reflection hump less pronounced, since photoelectric absorption by the lighter elements no longer occurs in the low-energy band (Ross & Fabian 1993). This is consistent with the lack of a strong reflection hump (Iwasawa et al. 1995; Smith & Done 1995). The disc-line model of the rest 6.7-keV line can also account for the observed line profile with the smaller inclination of $i \sim 36°$.

The line profile from the ionized disc may not be a single disc-line shape, but might be a multiple line complex, as shown by Matt et al. (1993). The ionization parameter,

$\xi = L/nR^2$ (Kallman & McCray 1982), which is high ($\xi \sim 1000$) at the smaller radii of the disc, declines sharply as a function of radius. Consequently, the observed line shape is composed of an ionized line from the inner part and less-ionized lines from outer parts. The disc-line model of He-like iron describes the 4.6 and 6.8 keV horns, and the other emission-line-like feature across the intermediate energy (such as the 5.6-keV peak) could be from less-ionized matter.

However, if the reflection matter is highly ionized, a deep iron K absorption edge should be observed as seen in the *Ginga* spectra of Galactic black hole candidates (Ebisawa 1991). The reflection below the edge energy becomes quite efficient, since lighter elements, which absorb the reflected radiation in the energy band, have been fully stripped. This causes the iron K edge feature evident in a sum of the incident and reflected spectra (Ross, Fabian & Brandt 1995). However, the *Ginga* spectrum of this object shows no strong evidence for such a deep edge, and the fit with a sharp edge at threshold energy of 8.8 keV appropriate to He-like iron gives an optical depth smaller than 0.27 (Iwasawa et al. 1995; Smith & Done 1995). Moreover, a broadened edge model (Ebisawa 1991), which is expected from an accretion disc, does not improve the quality of the fit. The ionized disc thus does not match the spectrum of this object.

Another significant difference in IRAS 18325 − 5926 is the steep X-ray continuum. In the combined *Ginga* sample of Awaki (1991) and Nandra (1991) and the *EXOSAT* data of Turner & Pounds (1989), this object has the steepest 2–10 keV continuum. We have verified the steep spectrum with *ASCA*, and confirm that the continuum shape is a stable property of this object. The only broad-line object published with a steeper spectral slope is the quasar PKS 0558 − 504 (Remillard et al. 1991). While the origin of the X-ray continuum is unknown, the relatively small range of the 2–10 keV spectral index of Seyfert 1 galaxies is almost a defining characteristic. The situation with Seyfert 2 objects is less well determined, but they tend, in the *Ginga* and *ASCA* data, to have relatively flat spectra (Awaki et al. 1991; Iwasawa et al. 1994; Ueno et al. 1994) and show large absorption. The rapid variability of the continuum shows that we are observing this object directly and not via scattered radiation, as is thought to be the case for Seyfert 2 objects. The lack of the cold reflection signatures suggests that the putative molecular/dust torus must be Thomson-thin, or that the solid angle of the optically thick part is small (Iwasawa et al. 1995), or that the iron abundance is supersolar as discussed above. It thus seems that perhaps IRAS 18325 − 5926 is, on the basis of its X-ray properties, a somewhat different class of object. Narrow-line Seyfert 1 objects show steep X-ray spectra as well as rapid X-ray variability (e.g. Boller, Brandt & Fink 1996). IRAS 18325 − 5926 shares the X-ray properties of this class, except for its large absorption. In the optical band, its emission-line spectrum (Carter 1984; Iwasawa et al. 1995) does not fit the characteristic signatures of narrow-line Seyfert 1 objects, e.g. [O iii] $\lambda 5007/H\beta < 3$ and a relatively large optical Fe ii/Hβ ratio. If heavy obscuration masks the optical characteristics of the inner nucleus and thereby hides the Fe ii emission and much of the Hβ emission, it may be possible that a narrow-line Seyfert 1 nucleus lies in IRAS 18325 − 5926.

5   CONCLUSIONS

We have shown that the Fe K line from IRAS 18325 − 5926 is very strong and broad, and that its shape is consistent with a disc-line model. The line profile has a blue peak at the rest-energy 6.9 keV, significantly higher than the 6.4 keV which is observed in most active galaxies. The shifts of the line to blue and red suggest a large inclination of the accretion disc. Non-solar abundances are needed to account for the large equivalent width. A picture in which the Fe K line originates in a highly ionized disc is also consistent with the observed line shape, line strength and the absence of a reflection 'hump', but the lack of deep iron K edge is not compatible with this picture. We have confirmed that the observed spectral index in the 2–10 keV range is steeper than that of any other active galaxy. Spectral variability is found in the soft X-ray band below 1 keV, which suggests an extended component outside the nuclear obscuration. The combination of a strong, broad Fe line, steep continuum and rapid variability is unique amongst the well-observed AGN and is rather different from that expected from its optical classification as a Seyfert 2 galaxy.

REFERENCES

Anders E., Grevesse N., 1989, Geochim. Cosmochim. Acta, 53, 197
Awaki H., 1991, PhD thesis, Univ. Nagoya, Japan
Awaki H., Koyama K., Inoue H., Halpern J. P., 1991, PASJ, 43, 195
Awaki H. et al., 1994, PASJ, 46, L65
Boller Th., Brandt W. N., Fink R., 1996, A&A, 305, 53
Brindle C., Hough H., Baily J. A., Axon D. J., Ward M. J., Sparks W. B., McLean I. S., 1990, MNRAS, 244, 577
Brinkmann W. et al., 1994, A&A, 288, 433
Carter D., 1984, Astron. Express, 1, 61
Chen K., Halpern J. P., Fillipenko A. V., 1989, ApJ, 339, 742
de Grijp M. H. K., Miley G. K., Lub J., de Jong T., 1985, Nat, 314, 240
Ebisawa K., 1991, PhD thesis, Univ. Tokyo, Japan
Fabbiano G., Kim D.-W., Trinchieri G., 1992, ApJ, 80, 531
Fabian A. C., Rees M. J., Stella L., White N. E., 1989, MNRAS, 238, 729
Fabian A. C., Nandra K., Brandt W. N., Hayashida K., Makino F., Yamauchi M., 1994, in Makino F., Ohashi T., eds, New Horizon of X-Ray Astronomy. University Academy Press, Tokyo, p. 573
Fabian A. C., Nandra K., Reynolds C. S., Brandt W. N., Otani C., Tanaka Y., Inoue H., Iwasawa K., 1995, MNRAS, in press
Fiore F., Elvis M., McDowell J. C., Siemiginowska A., Wilkes B. J., 1994, ApJ, 431, 515
Gendreau K. C. et al., 1995, PASJ, 47, L5
George I. M., Fabian A. C., 1991, MNRAS, 249, 352
Ghisellini G., George I. M., Fabian A. C., Done C., 1991, MNRAS, 248, 14
Guilbert P. W., Rees M. J., 1988, MNRAS, 233, 475
Haardt F., 1993, ApJ, 413, 680
Iwasawa K., Yaqoob T., Awaki H., Ogasaka Y., 1994, PASJ, 46, L167
Iwasawa K., Kunieda H., Tawara Y., Awaki H., Koyama K., Murayama T., Taniguchi Y., 1995, AJ, 110, 551
Kallmann T. R., McCray R., 1982, ApJS, 50, 623
Koyama K., 1992, in Brinkmann W., Trümper J., eds, MPE Report 235, X-ray Emission from Active Galactic Nuclei and the Cosmic X-ray Background. p. 74
Laor A., 1991, ApJ, 376, 90
Lightman A. P., White T. R., 1988, ApJ, 335, 57
Loewenstein M., Mushotzky R. F., Tamura T., Ikebe Y., Makishima K., Matsushita K., Awaki H., Serlemitsos P. J., 1994, ApJ, 436, L75
Makishima K. et al., 1994, PASJ, 46, L77
McCammon D., Sanders ?., 1990, ARA&A, 28, 657
Matt G., Perola G. C., Piro L., 1991, A&A, 247, 25
Matt G., Perola G. C., Piro L., Stella L., 1992, A&A, 257, 63
Matt G., Fabian A. C., Ross R. R., 1993, MNRAS, 262, 179
Mulchaey J. S., Mushotzky R. F., Weaver K. A., 1992, ApJ, 390, L69
Mulchaey J. S., Corbett C., Wilson A. S., Mushotzky R. F., Weaver K. A., 1993, ApJ, 414, 144
Mushotzky R. F., Done C., Pounds K. A., 1993, ARA&A, 31, 717
Mushotzky R. F., Fabian A. C., Iwasawa K., Kunieda H., Matsuoka M., Nandra K., Tanaka Y., 1995, MNRAS, 273, L9
Nandra K., 1991, PhD thesis, Univ. Leicester
Nandra K., Pounds K. A., 1994, MNRAS, 268, 405
Pfeffermann E. et al., 1987, Proc. SPIE, 733, 519
Remillard R. A., Grossan B., Bradt H. V., Ohashi T., Hayashida K., Makino F., Tanaka Y., 1991, Nat, 350, 589
Reynolds C. S., Fabian A. C., Inoue H., 1995, MNRAS, 276, 1311
Ross R. R., Fabian A. C., 1993, MNRAS, 261, 74
Ross R. R., Fabian A. C., Brandt W. N., 1995, MNRAS, in press
Shakura N. I., Sunyaev R. A., 1973, A&A, 24, 337
Smith D. A., Done C., 1995, MNRAS, in press
Tanaka Y., Inoue H., Holt S. S., 1994, PASJ, 46, L37
Tanaka Y. et al., 1995, Nat, 375, 659
Trümper J., 1983, Adv. Space Res., 4, 241
Turner T. J., Pounds K. A., 1989, MNRAS, 240, 833
Turner T. J., George I. M., Mushotzky R. F., 1993, ApJ, 412, 72
Ueno S., Mushotzky R. F., Koyama K., Iwasawa K., Awaki H., Hayashi I., 1994, PASJ, 46, L71
Ward M. J., Done C., Fabian A. C., Tennant A. F., Shafer R. A., 1988, ApJ, 324, 767
Weaver K. A. et al., 1994, ApJ, 423, 621
Zdziarski A. A., Fabian A. C., Nandra K., Celotti A., Rees M. J., Done C., Coppi P. S., Madjeiski G. M., 1994, MNRAS, 269, p55
Życki P. T., Czerny 1994, MNRAS, 266, 653